PCCP

Intramolecular boron-locking strategy induced the remarkable first hyperpolarizability

Journal:	*Physical Chemistry Chemical Physics*
Manuscript ID	CP-ART-12-2023-006276.R1
Article Type:	Paper
Date Submitted by the Author:	27-Feb-2024
Complete List of Authors:	Li, Bo; Guizhou Education College, Guizhou Provincial Key Laboratory of Computational Nano-Material Science Lin, Shichen; Kyushu University, Interdisciplinary Graduate School of Engineering Sciences Gu, Fenglong; MOE Key Laboratory of Environmental Theoretical Chemistry, South China Normal University, School of Environment

Journal Name

ARTICLE TYPE

Cite this: DOI: 00.0000/xxxxxxxxxx

Intramolecular boron-locking strategy induced the remarkable first hyperpolarizability: role of torsion angles between donor and acceptor units

Bo Li,[a] Shichen Lin,[b] and Feng Long Gu*[c,d]

Received Date
Accepted Date

DOI: 00.0000/xxxxxxxxxx

In the conventional strategy to design donor–acceptor (D–A) organic molecules for the large electronic contribution part to first hyperpolarizability (β), the effects of the torsion angles (θ_1 and θ_2) between donor and acceptor moieties are barely considered. To address this issue, in this work, an promising and novel intramolecular boron-locking strategy combined with different locking groups of different acceptors to control the θ_1 and θ_2 has been proposed thereby to make D–A organic molecules for the large β values. Intriguingly, reducing the torsion angles will make the β value of pyridiny thiophene units triphenylamine (Py–Th–TPA) dramatically up to 94%, which mainly ascribes to that smaller θ_1 and θ_2 lead to lower excited energy of the crucial excited state, and then enhanced charge transfer (CT) from TPA to Py–Th moieties, and finally greatly increase the donor and acceptor parts contributions to β. Correlation between the difference, $|\theta_1 - \theta_2|$, and β hold large coefficient of determination, R^2=0.78, which demonstrates that $|\theta_1 - \theta_2|$ can be regarded as a potential descriptor for designing NLO materials with D–A architecture. Clearly, we uncovered that θ_1 and θ_2 play a crucial role for performance of NLO materials with D–A fragment.

1 Introduction

Recent years, in the field of nonlinear optics (NLO), it has witnessed much attention focusing on designing high performance NLO materials to meet growing requirements of practical applications of dynamic image processing, optical frequency conversion and data storage[1–9]. Great efforts have been put into designing NLO materials with large hyperpolarizabilities, consequently, some effective approaches to enhance hyperpolarizabilities have been proposed up to date[2,10,11]. In terms of those effective approaches to enhance hyperpolarizatilities, constructing organic molecules with D–A architecture has been emerged as a vibrant topic[6–9,12–14]. Moreover, it has been confirmed that inherent NLO properties, such as the first hyperpolarizability, are closely related to torsion angles between donor and acceptor moieties, which demonstrates that controlling torsion angles between donor and acceptor units has become a key factor for obtaining high performance NLO materials[8,9,15–17]. To data, it is still an open issue to find a robust approach to control torsion angles to achieve the goal with high performance NLO materials.

Recently, strategies to design high performance NLO materials by controlling torsion angles between donor and acceptor fragments have been proposed[8,9,15–17]. For instance, installing large groups into donor and acceptor units has been proposed by Lou and co-workers[15–17], which is using steric hindrance of large groups to regulate torsion between donor and acceptor moieties. However, large groups are difficult to be inserted into donor and acceptor fragments to make small torsion angles between donor and acceptor units. Importantly, large hyperpolarizabilities of D–A organic molecules commonly corresponds to small torsion angles[9]. Fortunately, our previous work[8,9] have reported that intramolecular carbon-locking strategy can be served as an effective strategy for getting small torsion angles between donor and acceptor moieties, thereby predicting a series of candidates of NLO materials with large hyperpolarizabilities. But, those candidates of NLO materials found by our previous work are lack of strong intramolecular/intermolecular noncovalent interactions (INCIs), which is the key for stability. Therefore, it is urgent to find a better strategy with torsion angles between donor and acceptor fragments controllable, and with high stability as well, for high performance NLO materials.

Recent studies have indicated that INCIs can enhance the character of charge transfer (CT) from the donor to the acceptor[18–20]. And strong CT character is conducive to generating desirable

[a] Guizhou Provincial Key Laboratory of Computational Nano-Material Science, Guizhou Education University, Guiyang 550018, P. R. China
[b] Interdisciplinary Graduate School of Engineering Sciences, Kyushu University, 6-1 Kasuga-Park, Fukuoka 816-8580, Japan
[c] MOE Key Laboratory of Environmental Theoretical Chemistry, South China Normal University, Guangzhou 510006, P. R. China, E-mail: gu@scnu.edu.cn
[d] SCNU Environmental Research Institute, Guangdong Provincial Key Laboratory of Chemical Pollution and Environmental Safety, School of Environment, South China Normal University, Guangzhou 510006, P. R. China.

factors for obtaining large hyperpolarizabilities[8]. Moreover, intermolecular noncovalent interactions were also found to play important role in NLO properties, and can be served as efficient strategy for designing NLO materials[21,22]. For instance, the first hyperpolarizability values of complexes formed by INCIs are much larger than the corresponding to isolated systems[22]. Furthermore, large bulky nature of donor and acceptor endows congenital factors for forming INCIs. As above mentioned, intramolecular locking strategy combined with INCIs may be served as a promising and novel strategy for developing high performance NLO materials with D–A architecture. Therefore, thermally activated delayed fluorescence candidate of pyridiny thiophene units triphenylamine (Py–Th–TPA)[23] (as shown in Fig. 1) with large bulky character is selected as the study subject in this work, as well as the intramolecular boron-locking strategy combined with different acceptor groups (R groups are listed in Fig. 1) interacting to Py–Th–TPA is presented. The results of INCIs between locking groups (R) and donor (TPA)/acceptor (Py–Th), the CT from TPA to Py–Th units, and the first hyperpolarizability (β) are reported.

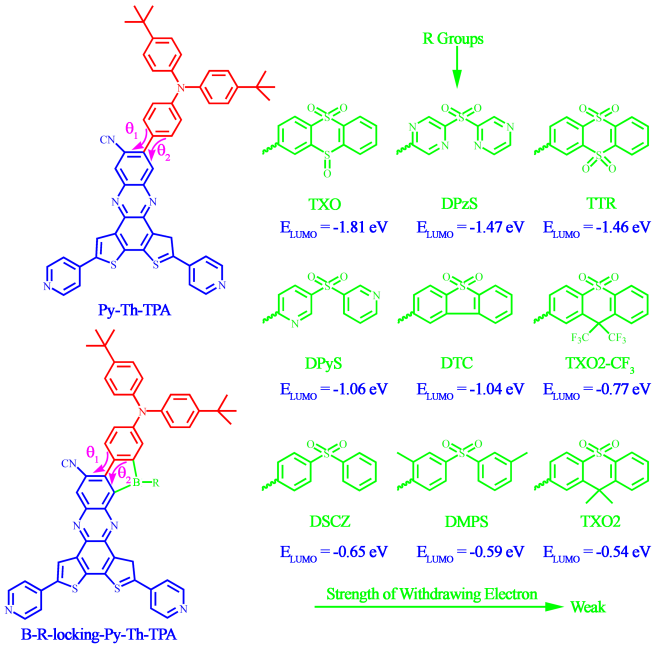

Fig. 1 The geometries of Py-Th-TPA and B–Rlocking–Py–Th–TPA, and torsion angles (θ_1 and θ_2) between donor and acceptor moieties, where R groups include TXO, DPzS, TTR, DPyS, DTC, TXO2-CF_3, DSCZ, DMPS and TXO2, and acceptor units (blue and green parts) are Py-Th and R groups, and donor (red part) corresponding to TPA fragment.

2 Computational details

The geometric optimizations and frequency calculations of all geometries of Fig. 1 are performed by M06-2X-D3/def2-SVPP level[24–27] as well as SMD continuum solvation model[28] combination with toluene solvent. Furthermore, it is worthy noting that long-range-corrected functional CAM-B3LYP[29] has displayed good robust for calculating excited state properties of excited energy (ΔE), transition dipole moment ($\Delta\mu$) and hyperpolarizabilities[3–5]. As a consequence, CAM-B3LYP/def2-SVPP level[27,29] is utilized to calculate ΔE and $\Delta\mu$, while CAM-B3LYP/Jul-cc-pVDZ[29–31] level is used to calculate electronic contribution part to the first hyperpolarizability (β). And β is obtained by equation 1.

$$\beta = (\beta_x^2 + \beta_y^2 + \beta_z^2)^{\frac{1}{2}} \tag{1}$$

with

$$\beta_i = \beta_{iii} + \beta_{ijj} + \beta_{ikk} \tag{2}$$

where $i, j, k \in \{x, y, z\}$ in equation 2.

The first hyperpolarizability density $\{\rho_{ij}^{(2)}(r)\}$[32] of characterizing electron densities contribution to β reflects that electron densities distribution of spatial point r under an uniform external electric field (F),

$$\rho_{ij}^{(2)}(r) = \frac{\partial^2 \rho(r)}{\partial F^2}|_{F=0} = \frac{\rho(F) - 2\rho(0) + \rho(-F)}{F^2} \tag{3}$$

with

$$\beta_{ijk} = \frac{1}{2!}\int r_i \rho_{jk}^{(2)}(r) dr \tag{4}$$

where $i = j \in \{x, y, z\}$ in equation 3, and $i = j = k \in \{x, y, z\}$ in equation 4.

Furthermore, energy decomposition analysis is done by B3LYP/def2-TZVP[27,33] level and sobEDA[34] combination with Multiwfn(Revision 3.8dev), where B-R-locking-Py-Th-TPA is divided into two fragments, namely, Py-Th-TPA and B-R units. The sobEDA method is defined as follow:

$$\Delta E_{\text{int}} = \Delta E_{\text{els}} + \Delta E_{\text{x}} + \Delta E_{\text{rep}} + \Delta E_{\text{orb}} + \Delta E_{\text{DFTc}} + \Delta E_{\text{dc}} \tag{5}$$

where $\Delta E_{\text{x}} + \Delta E_{\text{rep}}$ denotes exchange-repulsion term, ΔE_{orb} represents orbital interaction term, and $\Delta E_{\text{DFTc}} + \Delta E_{\text{dc}}$ is Coulomb correlation term, the more details about sobEDA method can be found in original literature[34].

The above calculations are carried out by Gaussian 16 package (Revision B.01)[35]. $\Delta\mu$, multi-level analysis[36,37], the first hyperpolarizability density analysis and decomposition analysis, the distributions of electron and hole[38], the independent gradient model (IGM)[39] based on Hirshfeld partition of molecular density (IGMH)[40], integrating of $-x\rho_{xx}^{(2)}(r)$ function by multi-center numerical integration algorithm proposed by Becke[41] are executed by open-access, powerful functions and user-friendly Multiwfn program (Revision 3.8dev)[42]. The isosurface diagrams of the first hyperpolarizability density are plotted by VMD[43] combination with Multiwfn (Revision 3.8dev).

3 Results and discussion

Geometries of Py–Th–TPA and B–R–locking–Py–Th–TPA obtained by M06-2X-D3/def2-SVPP level are illustrated in Fig. 1, where R groups are composed of the different acceptors of TXO, DPzS, TTR, DPyS, DTC, TXO2-CF_3, DSCZ, DMPS and TXO2. Interestingly, one found that there are remarkable folded phenomenon in R groups of DPzS, DPyS, TXO2-CF_3 and DMPS, which is conductive to forming INCIs of $\pi\cdots\pi$ between R groups (DPzS, DPyS, TXO2-CF_3 and DMPS) and acceptor unit (Py–Th). Compared with B–R–locking–Py–Th–TPA, one also found from Table 1 that θ_1 and θ_2 (where θ_1 and θ_2 are remarked in Fig. 1) in Py–Th–TPA

Table 1 values of θ_1, θ_2 and $|\theta_1-\theta_2|$ (°) in Py–Th–TPA and B–locking–R–Py–Th–TPA, and dispersion interaction (E_{disp}, kcal/mol) between R groups and donor/acceptor, where R=TXO, DPzS, TTR, DPyS, DTC, TXO2-CF_3, DSCZ, DMPS and TXO2.

Compounds	θ_1	θ_2	$\lvert\theta_1-\theta_2\rvert$	E_{disp}
Py–Th–TPA	45.69	42.89	2.80	
R=TXO	0.57	0.88	0.31	–50.36
R=DPzS	2.04	1.42	0.62	–50.25
R=TTR	1.19	1.21	0.02	–49.25
R=DPyS	1.87	1.18	0.69	–51.45
R=DTC	0.26	0.50	0.24	–49.23
R=TXO2-CF_3	0.80	1.07	0.27	–55.20
R=DSCZ	0.76	0.05	0.71	–46.50
R=DMPS	0.67	0.08	0.59	–58.71
R=TXO2	2.17	0.60	1.57	–47.61

are dramatically decreased by intramolecular boron-locking strategy, namely, θ_1 and θ_2 decreasing from 45.69° to 0.26° and from 42.89° to 0.50°, respectively. What's more, it has been confirmed that inherent properties are closely related to torsion angles between donor and acceptor units[9]. As a consequence, the changes of θ_1 and θ_2 will cause that the inherent property of β has remarkable variation.

It is worth noting that there exist INCIs between R groups and donor (TPA)/acceptor (Py–Th) units. The visual analysis measure of IGMH is utilized to characterize INCIs in B–R–locking–Py–Th–TPA. As shown in Fig. 2, these INCIs are composed of $\pi\cdots\pi$, N···H, O···H, F···H, and these values of dispersion interaction (E_{disp}, seeing Table 1) range from –46.50 kcal/mol to –58.71 kcal/mol. These strong INCIs are beneficial to enhance thermal stability of B–R–locking–Py–Th–TPA, and can result in limited geometric deformations in excited state, thereby bringing small excited energy of the crucial excited state, which is beneficial to facilitate CT from donor (TPA) transfer to acceptor (Py–Th) fragments.

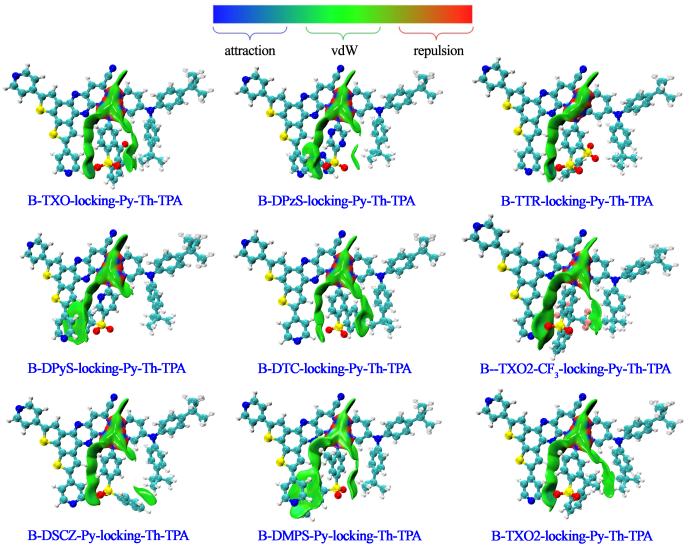

Fig. 2 The IGMH diagrams between R groups and donor (TPA)/acceptor (Py–Th) units in B–R–locking–Py–Th–TPA, where R=TXO, DPzS, TTR, DPyS, DTC, TXO2-CF_3, DSCZ, DMPS and TXO2.

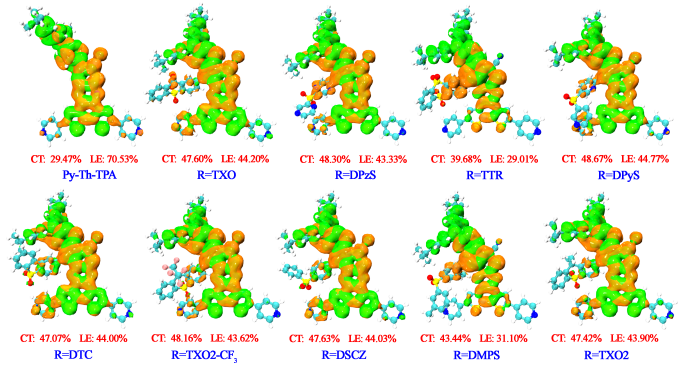

Fig. 3 The distributions of electron and hole of the crucial excited state in Py–Th–TPA and B–R–locking–Py–Th–TPA, and the ratios of CT from donor (TPA) transfer to acceptor (Py–Th) units and the ratios of local excitation (LE) in TPA and Py–Th, where orange and green denote electron and hole, respectively, where R=TXO, DPzS, TTR, DPyS, DTC, TXO2-CF_3, DSCZ, DMPS and TXO2.

In order to more intuitively analyze that INCIs impact on CT characters, the analysis approach of electron and hole analysis has been utilized to characterize CT characters of the crucial excited state in Py–Th–TPA and B–R–locking–Py–Th–TPA. And the crucial excited state is selected via multi-level analysis approach obtained by sum-of-states[36,37], namely, $\beta_{ZZZ}^{SOS}=6\sum_{i\neq j}(\frac{(\mu_{0i}^Z)^2\Delta\mu_i^Z}{\Delta E_i^2})+2\frac{\mu_{0i}^Z\mu_{0j}^Z\mu_{ij}^Z\Delta\mu_i^Z}{\Delta E_i\Delta E_j}+\frac{(\mu_{0j}^Z)^2\Delta\mu_j^Z}{\Delta E_j^2})$, where Z are one of the x, y and z direction, ΔE_i and ΔE_j corresponds to the excited energies of the i-th and j-th excited states, respectively; μ_{0i}^Z and μ_{0j}^Z represent components of the transition dipole moment from the ground to the excited states in the Z directions, μ_{ij} represents the transition dipole moment component in the Z direction from excited state i to excited state j, and $\Delta\mu_i^Z$ and $\Delta\mu_j^Z$ are the difference in Z directions between the dipole moment tensor for the excited state and the dipole moment tensor of the ground state, and the largest contribution to β_{ZZZ}^{SOS} origin from the n-th excited state is served as the crucial excited state. What's more, β_{ZZZ}^{SOS} is inversely proportional to ΔE, which indicates that ΔE is a one of decisive factors for taking control the magnitude of β.

The crucial excited state and the corresponding ΔE in B–R–locking–Py–Th–TPA corresponding to S8 with ΔE=3.68 eV for R=TXO, S8 with ΔE=3.69 eV for R=DPzS, S1 with ΔE=1.99 eV for R=TTR, S7 with ΔE=3.66 eV for R=DPyS, S7 with ΔE=3.69 eV for R=DTC, S7 with ΔE=3.64 eV for R=TXO2-CF_3, S7 with ΔE=3.67 eV for R=DSCZ, S1 with ΔE=2.13 eV for R=DMPS and S7 with ΔE=3.66 eV for R=TXO2, respectively, and the crucial excited state and ΔE value of Py–Th–TPA is S5 with ΔE=3.82 eV. It is worth noting that the crucial excited state of R=TTR and R=DMPS in B–R–locking–Py–Th–TPA have lower excited energy than another B–R–locking–Py–Th–TPA compounds, which owning to the crucial excited state of R=TTR and R=DMPS in B–R–locking–Py–Th–TPA all locate on the first excited state. Compared with the crucial excited state of Py–Th–TPA, it can be clearly seen from Fig. 3 that electron and hole of the crucial excited state in B–R–locking–Py–Th–TPA are obviously separated, and the ratios of CT from TPA transfer to Py–Th moieties are upped 10% to 18%, and the ratios of local excitation (LE) in TPA and Py–Th units are

decreased 26% to 31%, which demonstrates that CT character from TPA transfer to Py–Th fragment is obviously enhanced by INCIs. These results of electron and hole analysis directly suggest that INCIs between R groups and donor (TPA)/acceptor (Py–Th) are conducing to generating favorable factor of strong CT for obtaining large β value.

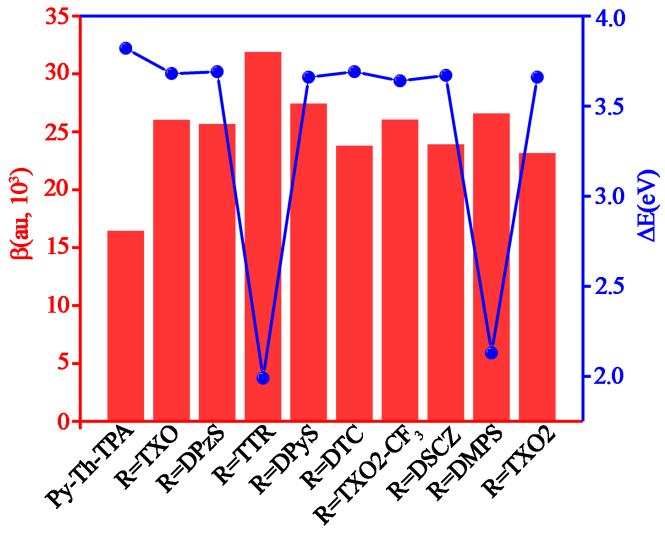

Fig. 4 β values (au) of Py–Th–TPA and B–R–locking–Py–Th–TPA obtained by CAM-B3LYP/Jul-cc-pVDZ level, and the relationship between β and excited energy (ΔE, eV) of the crucial excited state, where R=TXO, DPzS, TTR, DPyS, DTC, TXO2-CF_3, DSCZ, DMPS and TXO2.

These β values of Py–Th–TPA and B–R–locking–Py–Th–TPA obtained by CAM-B3LYP/Jul-cc-PvDZ level have been plotted Fig. 4, where the corresponding β values as follows: β =16462 au (β_{xxx} = 17214 au) for Py–Th–TPA, in B–R–locking–Py–Th–TPA, β =26038 au (β_{xxx} = 26659 au) for R=TXO, β =25688 au (β_{xxx} = 26222 au) for R=DPzS, β =31891 au (β_{xxx} = 32564 au) for R=TTR, β =27450 au (β_{xxx} = 28116 au) for R=DPyS, β =23800 au (β_{xxx} = 24431 au) for R=DTC, β =26054 au (β_{xxx} = 26945 au) for R=TXO2-CF_3, β =23922 au (β_{xxx} = 24597 au) for R=DSCZ, β =26599 au (β_{xxx} = 27052 au) for R=DMPS, β =231669 au (β_{xxx} = 24066 au) for R=TXO2. Excitingly, with dramatically decreasing of θ_1 and θ_2, it can be intuitively seen from Fig. 4 that β values of B–R–locking–Py–Th–TPA are significantly greater than β value of Py–Th–TPA, and the increased ratios of β of Py–Th–TPA range from 41% to 94%, which means that θ_1 and θ_2 hold obvious impact on β values, and intramolecular boron-locking strategy can also be served as an promising and novel strategy for increasing β value for twisted organic molecules with D–A architecture. Furthermore, these β values of Py–Th–TPA and B–R–locking–Py–Th–TPA hold same magnitude order compared with the reported candidates of high performance NLO materials of D–A organic molecules[8,9], which owning to following two reasons: firstly, TPA and Py–Th fragments retain strong strength of donating electron and withdrawing electron, respectively; secondly, heteroatom of Py–Th unit can enhance $\pi-$electron delocalization, thereby which results in large β value. Therefore, Py–Th–TPA and B–R–locking–Py–Th–TPA can be also served as potential candidates of high performance NLO materials.

To shed light on the mechanisms of increasing of β , the following analysis measures have been adopted. First of all, because large INCIs values and small θ_1/θ_2 lead to limited geometrical deformations in excited, which is conductive to generating strong CT character from TPA transfer to Py–Th fragments, thereby ΔE in Py–Th–TPA are obviously decreased (as depicted in Fig. 4), namely, ΔE from 3.82 eV (Py–Th–TPA) reduced to 1.99 eV (B–R–locking–Py–Th–TPA with R=TTR). And β is inversely proportional to ΔE[36,37], thereby ΔE becomes the mainly decisive factor for governing magnitude of β. Accordingly, the increasing of β value in Py–Th–TPA is caused by the decreasing of ΔE.

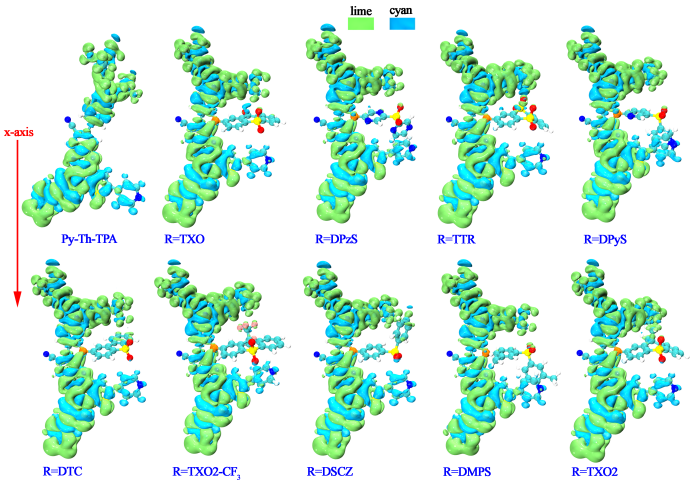

Fig. 5 The first hyperpolarizability density diagrams $\{-x\times\rho^2_{xx}(r)\}$ of Py–Th–TPA and B–R–locking–Py–Th–TPA, where lime and cyan denote the positive and negative contributions, respectively, where R=TXO, DPzS, TTR, DPyS, DTC, TXO2-CF_3, DSCZ, DMPS and TXO2.

Then, the first hyperpolarizability density approach of quantitative analysis is utilized to characterize spatial distributions of electron density contributions to β. It can be found from Fig. 5 that electron density contribution to β mainly distributed on Py–Th and TPA units, and electron density in Py–Th fragment mainly distributed on the same side as the cyano group. Furthermore, it is worth noting that electron density distributing on B–R group is almost negligible, which reflects that the effect of B–R groups on β is almost negligible. The first hyperpolarizability density analysis suggest that large INCIs values and small θ_1/θ_2 mainly impact the electron density distribution in donor and acceptor units.

To deeply figure out large INCIs values and small θ_1/θ_2 effect on β, the numerical contributions of three moieties of TPA donor, Py–Th acceptor and B–R groups to axial component of β_{xxx} are further obtained by utilizing the multi-center numerical integration algorithm[41] to integrate $-x\times\rho^2_{xx}(r)$ function, and the corresponding results have been plotted in Fig. 6. It can be intuitively seen from Fig. 6 that $\beta^{\text{Becke}}_{xxx}$ values of TPA and Py–Th units in Py–Th–TPA are obviously increased, while $\beta^{\text{Becke}}_{xxx}$ values of B–R groups are all small and negative values. Because large INCIs values and small θ_1/θ_2 enhanced CT character from TPA transfer Py–Th, which results in $\beta^{\text{Becke}}_{xxx}$ values of TPA and Py–Th fragments in Py–Th–TPA are significantly upped. In addition, small and negative $\beta^{\text{Becke}}_{xxx}$ values in B–R groups further confirm that θ_1 and θ_2

occupy an very important position for NLO materials composed of organic molecules with D–A fragment.

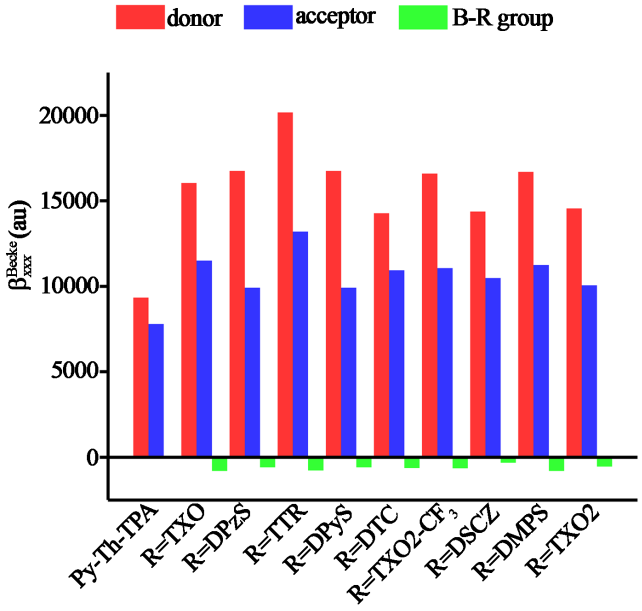

Fig. 6 The axial component of β_{xxx}^{Becke} for TPA, Py-Th and B-R fragments obtained by CAM-B3LYP/Jul-cc-pVDZ level, where red, blue and green denote donor (TPA), acceptor (Py-Th) and B–R groups, respectively, where R=TXO, DPzS, TTR, DPyS, DTC, TXO2-CF_3, DSCZ, DMPS and TXO2.

In general, structure–performance relationships pave an facial approach for evaluating the performance of NLO materials. Intriguingly, one found that the correlation between $|\theta_1 - \theta_2|$ and β have displayed linear correlation with coefficient of determination R^2=0.78 (Fig. 7(a)). At the same time, correlations between $|\theta_1 - \theta_2|$ and β values origin from donor and acceptor parts in Py–Th–TPA and B–R–locking–Py–Th-TPA have been obtained as well (Fig. 7(b-c)). One can clearly from Fig. 7(b-c) that good correlations have been found between $|\theta_1 - \theta_2|$ and β values origin from donor and acceptor, and hold coefficient of determination R^2 =0.77 (Fig. 7(b)) and R^2 =0.90 (Fig. 7(c)) corresponding to donor and acceptor moieties, respectively. These good correlations suggest that the difference of $|\theta_1 - \theta_2|$ locates on small regions is beneficial to generate total β value. Moreover, to further verify the correlations between $|\theta_1 - \theta_2|$ and $\beta/\beta_{xxx}^{Becke}$, these two points of Py–Th–TPA and R=TTR in B–R–locking–Py–Th–TPA are removed, the corresponding correlations results are provided in Fig. S1 in Supporting Information, and the coefficients of determination in between $|\theta_1 - \theta_2|$ and β_{xxx}^{Becke} have reached R^2 =0.60 for TPA fragment and R^2 =0.64 for Py-Th fragment, which further demonstrates that $|\theta_1 - \theta_2|$ is a rational descriptor for predicting the value of β. The above large R^2 values between $|\theta_1 - \theta_2|$ and β suggests that the difference of $|\theta_1 - \theta_2|$ can be served as proposing descriptor for designing NLO materials with D–A architecture, thereby inspiring chemists to put forward novel and desirable approaches for obtaining NLO materials with large β value. At the same time, the good correlation between $|\theta_1 - \theta_2|$ and β provides facile way for estimating β value of D–A architecture system.

Furthermore, Luis and coworkers[44–46] have confirmed that

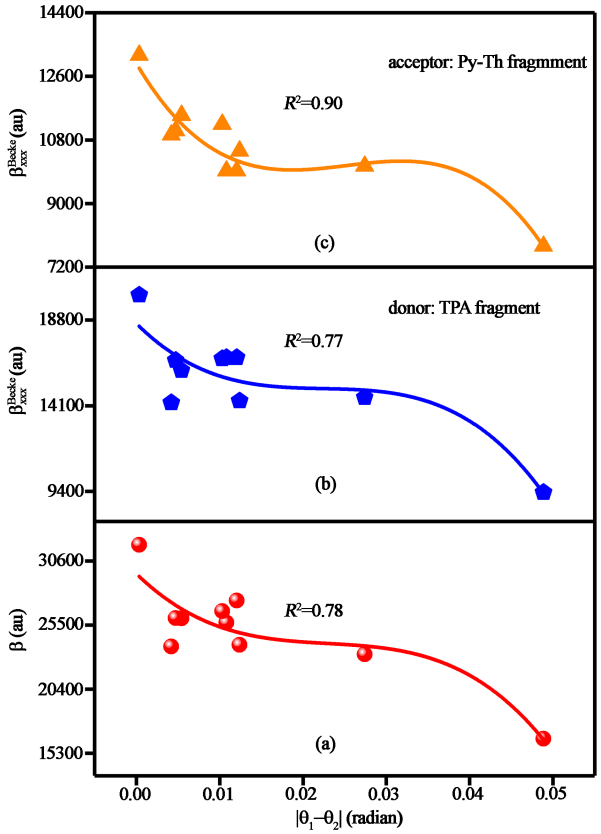

Fig. 7 Correlations between $|\theta_1 - \theta_2|$ and $\beta/\beta_{xxx}^{Becke}$, where coefficient of determination, (a) R^2 =0.78 for correlation between $|\theta_1 - \theta_2|$ and β in Py–Th–TPA and B–R–locking–Py–Th–TPA, (b) R^2 =0.77 for correlation between $|\theta_1 - \theta_2|$ and β_{xxx}^{Becke} in TPA fragment (donor part) of Py–Th–TPA and B–R–locking–Py–Th–TPA, and (c) R^2 =0.90 for correlation between $|\theta_1 - \theta_2|$ and β_{xxx}^{Becke} in Py–Th fragment (acceptor part) of Py–Th–TPA and B–R–locking–Py–Th–TPA, where R=TXO, DPzS, TTR, DPyS, DTC, TXO2-CF_3, DSCZ, DMPS and TXO2.

the nuclear relaxation contribution to the first hyperpolarizability (β^{nr}) is also a key component for measuring performance of NLO materials. Thus, β_{xxx}^{nr} values of Py–Th–TPA and B–R–locking–Py–Th–TPA in the direction of dipole moment are further calculated. These β_{xxx}^{nr} values of Py–Th–TPA and B–R–locking–Py–Th–TPA are: β_{xxx}^{nr} = 4148 au for Py–Th–TPA, β_{xxx}^{nr} = 5624 au for R= TXO, β_{xxx}^{nr} = 3394 au for R= DPzS, β_{xxx}^{nr} = 5030 au for R= TTR, β_{xxx}^{nr} = 6672 au for R= DPyS, β_{xxx}^{nr} = 3826 au for R= DTC, β_{xxx}^{nr} = 4835 au for R= TXO2-CF_3, β_{xxx}^{nr} = 5351 au for R= DSCZ, β_{xxx}^{nr} = 4603 au for R= DMPS, β_{xxx}^{nr} = 5812 au for R= TXO2. Compared with β_{xxx}^{nr} of Py–Th–TPA, the variation ratios of β_{xxx}^{nr} of B–R–locking–Py–Th–TPA range from −7.7% to 60.8%. While the variation ratios of electronic contribution part β_{xxx} values of B–R–locking–Py–Th–TPA range from 39.8% to 89.2%. The variation ratios of β_{xxx} and β_{xxx}^{nr} demonstrate that the effect of θ_1 and θ_2 on β_{xxx} is more obvious compared with β_{xxx}^{nr}.

4 Conclusions

In summary, based on utilizing intramolecular boron-locking strategy combination with different acceptor groups (R=TXO, DPzS, TTR, DPyS, DTC, TXO2-CF_3, DSCZ, DMPS and TXO2) to

modify β value of Py-Th–TPA, and then investigating geometric and electronic properties of B–R–locking–Py–Th–TPA in this work. Several key findings are highlighted as follow:

(i) These INCIs ($\pi\cdots\pi$, N$\cdots$H, O$\cdots$H and F$\cdots$H) between R groups and donor (TPA)/acceptor (Py–Th–TPA) moieties are conductive to enhancing thermal stability of B–R–locking–Py–Th–TPA, and decreasing excited energy of the crucial excited state, thereby enhancing CT from donor (TPA) transfer to acceptor (Py–Th) units.

(ii) Torsion angles (θ_1 and θ_2) between donor and acceptor moieties hold very important position in performance of NLO materials. And the difference of $|\theta_1 - \theta_2|$ can be served as a potential descriptor for designing NLO materials with D–A architecture.

(iii) Intramolecular boron-locking strategy can be served as a promising and novel strategy for enhancing β values of twisted D–A organic molecules.

Overall, these significant findings of this work have pointed out INCIs between locking groups and donor/acceptor units, torsion angles between donor and acceptor fragments all play pivotal role in NLO materials, and provided a robust foundation and a new type of molecular scaffold for designing high performance NLO materials with D–A architecture as well.

Conflicts of interest

There are no conflicts of interest to declare.

Acknowledgements

Dr. Bo Li is grateful for the financial support from the National Natural Science Foundation of China (NSFC Grant No. 22203019), the Scientific Research Projects of Higher Schools (Youth Projects) of Guizhou Provincial Department of Education (Grant No. QJJ(2022)253), the financial support from the Science Research Foundation of Guizhou Education University (Grant No. 2021BS026) and the Opening Research Foundation of MOE Key Laboratory of Environmental Theoretical Chemistry for South China Normal University (Grant No. 20210101). Mr. Shichen Lin thanks the financial support from the Japan Science and Technology Agency program "Support for Pioneering Research Initiated by the Next Generation" (JST SPRING, Grant Number JPMJSP2136).

Notes and references

1 Y. Shi, D. Frattarelli, N. Watanabe, A. Facchetti, E. Cariati, S. Righetto, E. Tordin, C. Zuccaccia, A. Macchioni and S. L. Wegener, *J. Am. Chem. Soc.*, 2015, **137**, 12521–12538.
2 S. Semin, X. Li, Y. Duan and T. Rasing, *Adv. Opt. Mater.*, 2021, **9**, 2100327.
3 B. Li, P. Sathishkumar, F. L. Gu and C. Zhu, *J. Phys. Chem. A*, 2020, **124**, 955–965.
4 B. Li, P. Sathishkumar and F. L. Gu, *Phys. Chem. Chem. Phys.*, 2021, **23**, 8489–8499.
5 B. Li, H. Shen, M. Deng and F. L. Gu, *J. Phys. Chem. Lett.*, 2022, **13**, 412–418.
6 Y. Yao, H.-L. Xu and Z.-M. Su, *J. Mater. Chem. C*, 2022, **10**, 12338–12349.
7 Y. Yao, H.-L. Xu and Z.-M. Su, *J. Mater. Chem. C*, 2022, **10**, 886–898.
8 B. Li, T. Xiao, H. Shen, M. Deng and F. L. Gu, *Phys. Chem. Chem. Phys.*, 2022, **24**, 21800–21805.
9 B. Li, T. Xiao, F. L. Gu, J. Jiang and C. Jia, *J. Phys. Chem. A*, 2023, **127**, 7274–7283.
10 M. Nakano and B. Champagne, *J. Phys. Chem. Lett.*, 2015, **6**, 3236–3256.
11 R.-L. Zhong, H.-L. Xu, Z.-R. Li and Z.-M. Su, *J. Phys. Chem. Lett.*, 2015, **6**, 612–619.
12 D. Zhang, W. Chen, J. Zou and J. Luo, *Chem. Mater.*, 2021, **33**, 3702–3711.
13 J.-T. Ye and Y.-Q. Qiu, *Phys. Chem. Chem. Phys.*, 2021, **23**, 15881–15898.
14 Y.-Y. Peng, B.-F. Li, P. Li, Y. Hou, B. Guo, Q. Yuan and W. Gan, *J. Phys. Chem. C*, 2022, **126**, 2234–2242.
15 A. J.-T. Lou, S. Righetto, C. Barger, C. Zuccaccia, E. Cariati, A. Macchioni and T. J. Marks, *J. Am. Chem. Soc.*, 2018, **140**, 8746–8755.
16 A. J.-T. Lou and T. J. Marks, *Acc. Chem. Res.*, 2019, **52**, 1428–1438.
17 A. J.-T. Lou, S. Benis, M. Gao, A. Baev, D. Kim, E. W. Van Stryland, D. J. Hagan and T. J. Marks, *J. Phys. Chem. C*, 2020, **124**, 5363–5370.
18 Y. H. Lee, S. Park, J. Oh, J. W. Shin, J. Jung, S. Yoo and M. H. Lee, *ACS Appl. Mater. Interfaces*, 2017, **9**, 24035–24042.
19 X.-L. Chen, J.-H. Jia, R. Yu, J.-Z. Liao, M.-X. Yang and C.-Z. Lu, *Angew. Chem., Int. Ed*, 2017, **56**, 15006–15009.
20 E. Spuling, N. Sharma, I. D. W. Samuel, E. Zysman-Colman and S. Bräse, *Chem. Commun.*, 2018, **54**, 9278–9281.
21 R. Zaleśny, R. W. Góra, H. Reis, J. M. Luis *et al.*, *Phys. Chem. Chem. Phys.*, 2018, **20**, 19841–19849.
22 A. Iglesias-Reguant, H. Reis, R. W. Góra, J. M. Luis, R. Zaleśny *et al.*, *Phys. Chem. Chem. Phys.*, 2020, **22**, 4225–4234.
23 C.-Z. Yang, Z.-H. Pan, K. Zhang, J.-W. Tai, C.-K. Wang, L. Ding, M.-K. Fung and J. Fan, *Mater. Horiz.*, 2023, **10**, 945–951.
24 Y. Zhao and D. G. Truhlar, *Theor. Chem. Acc.*, 2008, **120**, 215–241.
25 Y. Zhao and D. G. Truhlar, *Acc. Chem. Res.*, 2008, **41**, 157–167.
26 S. Grimme, J. Antony, S. Ehrlich and H. Krieg, *J. Chem. Phys.*, 2010, **132**, 154104.
27 F. Weigend and R. Ahlrichs, *Phys. Chem. Chem. Phys.*, 2005, **7**, 3297–3305.
28 A. V. Marenich, C. J. Cramer and D. G. Truhlar, *J. Phys. Chem. B*, 2009, **113**, 6378–6396.
29 T. Yanai, D. P. Tew and N. C. Handy, *Chemical Physics Letters*, 2004, **393**, 51–57.
30 R. A. Kendall, T. H. Dunning Jr and R. J. Harrison, *J. Chem. Phys.*, 1992, **96**, 6796–6806.
31 D. E. Woon and T. H. Dunning Jr, *J. Chem. Phys.*, 1994, **100**, 2975–2988.

32 S. Yamada, M. Nakano, I. Shigemoto and K. Yamaguchi, *Chem. Phys. Lett.*, 1996, **254**, 158–164.

33 A. D. Becke, *J. Chem. Phys.*, 1993, **98**, 5648–5652.

34 T. Lu and Q. Chen, *J. Phys. Chem. A*, 2023.

35 M. J. Frisch, G. W. Trucks, H. B. Schlegel, G. E. Scuseria, M. A. Robb, J. R. Cheeseman, G. Scalmani, V. Barone, G. A. Petersson, H. Nakatsuji, X. Li, M. Caricato, A. V. Marenich, J. Bloino, B. G. Janesko, R. Gomperts, B. Mennucci, H. P. Hratchian, J. V. Ortiz, A. F. Izmaylov, J. L. Sonnenberg, D. Williams-Young, F. Ding, F. Lipparini, F. Egidi, J. Goings, B. Peng, A. Petrone, T. Henderson, D. Ranasinghe, V. G. Zakrzewski, J. Gao, N. Rega, G. Zheng, W. Liang, M. Hada, M. Ehara, K. Toyota, R. Fukuda, J. Hasegawa, M. Ishida, T. Nakajima, Y. Honda, O. Kitao, H. Nakai, T. Vreven, K. Throssell, J. A. Montgomery, Jr., J. E. Peralta, F. Ogliaro, M. J. Bearpark, J. J. Heyd, E. N. Brothers, K. N. Kudin, V. N. Staroverov, T. A. Keith, R. Kobayashi, J. Normand, K. Raghavachari, A. P. Rendell, J. C. Burant, S. S. Iyengar, J. Tomasi, M. Cossi, J. M. Millam, M. Klene, C. Adamo, R. Cammi, J. W. Ochterski, R. L. Martin, K. Morokuma, O. Farkas, J. B. Foresman and D. J. Fox, *Gaussian16 revision B.01*, 2016, Gaussian Inc. Wallingford CT.

36 K. Sasagane, F. Aiga and R. Itoh, *J. Chem. Phys.*, 1993, **99**, 3738–3778.

37 T. Lu, *Multiwfn manual, version 3.8(dev), Section 3.200.8, available at http://sobereva.com/multiwfn*, accessed September 1, 2023.

38 Z. Liu, T. Lu and Q. Chen, *Carbon*, 2020, **165**, 461–467.

39 C. Lefebvre, G. Rubez, H. Khartabil, J.-C. Boisson, J. Contreras-García and E. Hénon, *Phys. Chem. Chem. Phys.*, 2017, **19**, 17928–17936.

40 T. Lu and Q. Chen, *J. Comput. Chem.*, **43**, 539–555.

41 A. D. Becke, *J. Chem. Phys.*, 1988, **88**, 2547–2553.

42 T. Lu and F. Chen, *J. Comput. Chem.*, 2012, **33**, 580–592.

43 W. Humphrey, A. Dalke and K. Schulten, *J. Mol. Graph.*, 1996, **14**, 33–38.

44 J. M. Luis, J. Martí, M. Duran, J. L. Andrés and B. Kirtman, *J. Chem. Phys.*, 1998, **108**, 4123–4130.

45 M. Torrent-Sucarrat, J. M. Anglada and J. M. Luis, *J. Chem. Theory and Comput.*, 2011, **7**, 3935–3943.

46 M. Garcia-Borràs, M. Solà, J. M. Luis and B. Kirtman, *J. Chem. Theory and Comput.*, 2012, **8**, 2688–2697.